Environmental Pollution 242 (2018) 718–727

Contents lists available at ScienceDirect

Environmental Pollution

journal homepage: www.elsevier.com/locate/envpol

Re-emission of legacy mercury from soil adjacent to closed point sources of Hg emission☆

Wei Zhu [a, 1], Zhonggen Li [a], Ping Li [a], Ben Yu [a], Che-Jen Lin [a, b, c], Jonas Sommar [a], Xinbin Feng [a, *]

[a] State Key Laboratory of Environmental Geochemistry, Institute of Geochemistry, Chinese Academy of Sciences, Guiyang 550081, China
[b] Center for Advances in Water and Air Quality, Lamar University, Beaumont, TX 77710, United States
[c] Department of Civil and Environmental Engineering, Lamar University, Beaumont, TX 77710, United States

ARTICLE INFO

Article history:
Received 26 March 2018
Received in revised form
1 July 2018
Accepted 1 July 2018
Available online 6 July 2018

Keywords:
Chlor-alkali plant
Polyvinyl chloride production
Legacy mercury
Mercury isotope signatures
Air-soil mercury flux
Mercury reemission

ABSTRACT

Mercury (Hg) emissions from point sources to air may disperse over long distance depending on Hg speciation in the plume. A significant fraction of Hg, particularly in its divalent forms, deposits locally and causes pollution to surrounding biomes. The objective of this study was to investigate (1) the historic Hg deposition to the immediate vicinity of an industrial complex that had intentional use of Hg (i.e., chlor-alkali and polyvinyl chloride production) for 5 decades until 2011, and (2) the Hg^0 re-emission from soil to air soon after the closure of the facility. The spatial distribution of near-ground Hg^0 vapor in air, soil Hg concentration and stable isotope ratio, air-soil Hg^0 flux and Hg^0 concentration in soil pore-gas were measured. It was found that the surrounding soils are severely contaminated with Hg due to the Hg release of the industrial complex, displaying soil Hg content up to 4.8 $\mu g\ g^{-1}$. A spatial trend of Hg mass dependent isotope fractionation signature ($\delta^{202}Hg = -2.11‰$ to 0.72‰) with respect to the distance from the closed facility was identified, representing a mixing between regional background and industrial Hg sources. Hg release from the industrial operation enhanced surface soil Hg content within a 6.5-km radius from the facility. Inside the facility, residual Hg wastes (i.e., electrolysis sludge and consumed $HgCl_2$ catalyst) represent a strong localized emission source of atmospheric Hg^0. Near-ground atmospheric Hg^0 concentration and soil Hg^0 efflux progressively elevated toward the facility with an increase by 2–3 orders of magnitude compared to the values observed in the off-site background. These results suggest that the natural soil surfaces surrounding the closed industrial facility act as a large nonpoint source emitting legacy deposited Hg as much as the release from naturally enriched mines.

1. Introduction

Mercury (Hg) is a potent neurotoxic pollutant ubiquitously distributed globally (Lindberg et al., 2007). Hg emission from anthropogenic sources is made up of gaseous elemental Hg (Hg^0), gaseous oxidized Hg (GOM), and particulate bound Hg (PBM), while emission from natural surfaces is predominantly Hg^0 (Gustin, 2011). Once released into the atmosphere, GOM and PBM are readily deposited through wet and dry processes while Hg^0 is subject to long-range transport (Lindberg et al., 2007; Schroeder and Munthe, 1998). Deposited Hg can be reemitted back into the atmosphere by volatilization following biotic and abiotic reduction processes occurring in the natural substrates (Carpi and Lindberg, 1997; Fritsche et al., 2008). Globally, the increased anthropogenic emission has enriched soils and sediments with Hg by a factor of 3–4 in magnitude since pre-industrial times (Amos et al., 2015). The enrichment factor can be up to thousands of times higher at locations near the industrial sources (Biester et al., 2002).

Intentional use of Hg in industrial activities (e.g., chlor-alkali industry and artisanal gold mining) contribute to ~44% of total anthropogenic Hg emission (AMAP/UNEP, 2013). In chlor-alkali production, liquid elemental Hg has been widely used in the electrolytic cells. Fugitive Hg losses can occur through volatilization, discharge of wastewater, disposal of brine sludge waste resulting in contamination and severe enrichment of Hg in local air, water, soil

☆ This paper has been recommended for acceptance by Dr. Jorg Rinklebe.

* Corresponding author.
E-mail addresses: zhuweicas@gmail.com (W. Zhu), fengxinbin@vip.skleg.cn (X. Feng).

[1] Present address: Department of Forest Ecology and Management, Swedish University of Agricultural Sciences, SE-90183 Umeå, Sweden.

https://doi.org/10.1016/j.envpol.2018.07.002
0269-7491/

and sediments (Biester et al., 2002; Grangeon et al., 2012; Hissler and Probst, 2006; Kinsey et al., 2004a; Lindberg and Turner, 1977; Ullrich et al., 2007; Wängberg et al., 2003; Zhu et al., 2018). Strong Hg^0 emission from chlor-alkali plants (CAP) have been reported. An emission rate of 400–600 g Hg day^{-1} was observed from an active CAP in the southern US (Kinsey et al., 2004b; Southworth et al., 2004), while emission from 144 to 1296 g Hg day^{-1} during the investigation in European CAPs in Sweden and Italy (Grönlund et al., 2005). Intentionally use of $HgCl_2$ modified activated carbon (4.5–12% content by weight) in the carbide-based polyvinyl chloride (PVC) industry represented one of the largest global Hg demand (Pirrone et al., 2010). PVC industry has emerged as the largest Hg user in China, accounted for over 60% annual Hg demand (Lin et al., 2016). Recent inventory study on a Hg remover equipped PVC production line resulted in a release rate of 4.9 g Hg per tonne PVC to the environment (Ren et al., 2014).

"To protect human health and the environment from the adverse effects of mercury," the intergovernmental legal binding agreement *Minamata Convention for Mercury* aiming to reduce Hg emission and human/wildlife exposure has been signed in 2013 and entered into force in 2017 (UNEP Minamata Convention, 2014). Improvement of technology to reduce Hg emission and closure of point sources, therefore, are expected in the near future. Global anthropogenic Hg emission has declined by >30% since 1990, with the most pronounced reduction from North America and Europe (Zhang et al., 2016b). In addition to Hg emission reduction in major anthropogenic sources, such as coal-fired power plants by upgrading Hg removing technology (e.g., flue gas desulfurization, selective catalyst reduction, and activated carbon injection), phasing out and closure of smelting facilities (e.g., Pb/Zn smelters) and limiting the intentional use of Hg (e.g., in thermometers and chlor-alkali industry) help decrease Hg emissions from point sources. Nevertheless, large amounts of Hg have been deposited in the natural environment surrounding those point sources because of long-term release and accumulation of Hg during the industrial operation. However, little is known about the fate of Hg in the surrounding after the closure of a known point source of Hg emission from intentional Hg use. Owing to the bidirectional exchange characteristic of Hg^0 flux, soil can either receive deposition of atmospheric Hg^0 or emit Hg^0 depending on environmental conditions (e.g., vegetation, temperature, solar irradiation, soil moisture, microbial activities and ambient Hg^0 concentration etc.) (Zhu et al., 2016). Eckley et al. (2015) recently observed an elevated soil Hg^0 efflux after the closure of a large base-metal smelter in Canada. The fate and mobility of the historic deposited Hg in the surrounding of closed point sources is crucial for assessing remediation options. Lack of knowledge concerning the behavior of historic deposited Hg potentially hinders effective regulatory measures to curb its impact on the local area.

In this study, we measured *in situ* near-ground Hg^0 in air, air-soil Hg^0 flux and soil pore-gas Hg^0 concentration, as well as soil Hg contents and its stable Hg isotope ratios. The objectives of this study are to: (1) quantify the historic Hg deposition to the soil surrounding the closed industrial plant, (2) understand the spatial characteristics of atmospheric Hg^0 pollution and surface-air Hg^0 flux after the closure of the industrial plant in an attempt to understand the fate of legacy Hg in the environment media after the active release of Hg is stopped.

2. Experimental methods

2.1. Study area

The closed industrial plant (CIP), with integrated CAP and PVC production sectors (N 24.90°, E 102.46°, 1850m a.s.l., Fig. 1A) located in an industrial zone of ~7 Ha, 35 km west of Kunming City, the capital of Yunnan province in Southwestern China. The CIP is adjunct to the Anning city. The area subject to central Asia subtropical weather with prevailing wind from the southwest direction. The annual mean precipitation and temperature are 1000 mm and +14.9 °C, respectively. Soils surrounding the CIP is typical tropical latosol. Corresponding soil SiO_2/Al_2O_3 and organic matter content are 2.2–2.3 and 2%–3%, respectively (Tong et al., 2000).

Liquid elemental Hg and mercuric chloride were intentionally used in the facility from 1962 to its permanent closure in April 2011 for caustic soda, chlorine and PVC production, respectively. In March 2012, the natural agricultural surfaces surrounding the closed industrial facility (up to a distance of 11.5 km) and historic Hg contaminated sites (Hg cell room, brine sludge pile, and PVC workshop) were investigated including the air-surface Hg^0 flux and spatial distribution of ambient Hg^0 concentration via an integrated campaign (Fig. 1B). In the electrolytic cells, liquid elemental Hg was used as a cathode in the Castner-Kellner process (Kinsey et al., 2004a; Ullrich et al., 2007) during the period 1962–1991. After 1991, the Hg-free ion-selective membrane technique was implemented in separating sodium and chlorine electrolytically in the former Hg-cell room (~3000 m^2, Fig. 1C). The brine sludge, form by dumping electrolytic solid waste from the previously Hg cell room, was piled at the northeast side of the industrial zone, covering an area of ~1.1 hectares. From 1971 to April 2011, the chlorine gas produced by the CAP was used as feed for PVC production (~3×10^4 tons yr^{-1}) based on carbide processes. The position of the facility for PVC production is indicated in Fig. 1C as well as the sampling sites O1 and O2 in the administrative area located 420 m and 640 m west of the former Hg-cell room.

2.2. Ambient Hg^0 concentration and soil-air Hg^0 flux measurement

Ambient air Hg^0 concentration was measured at 12 sites, including 5 bare agricultural fields (A1-A5, Fig. 1B), two administrative offices located within the plant boundary (O1 and O2), two sites immediately inside and outside (<25 m distance) of the Hg-cell room (CI and CO) and the PVC workshop (PI and PO), and one at the base of piled brine sludge (BS, Fig. 1C). The ambient air Hg^0 at sites A1-A5, O1, O2, CI, and CO were measured using a Tekran® 2537B Hg vapor analyzer (cf. calibration details in the following paragraph) for 24 h. The highly elevated ambient air Hg^0 at PI, PO, and BS were measured for 8 h during daytime with a Lumex® RA-915 + portable Hg vapor analyzer. The Lumex instrument was calibrated by using the internal test cell prior to each sampling period (Zhu et al., 2013b). Ambient air intake was positioned at ~50 cm above the ground except for the five flux sampling sites (A1-A5, ~15 cm).

The bare soil surfaces at sites A1-A5 (Fig. 1B) located 0.75–11.5 km from the cell house were selected for Hg^0 flux measurement. At each site, Hg^0 flux was continuously sampled for 24 h using a semi-cylindrical quartz dynamic flux chamber (DFC, Ø 20 cm × 30 cm) coupled to a Tekran® 2537B instrument (Feng et al., 2005; Fu et al., 2012; Fu et al., 2008; Zhu et al., 2013a; Zhu et al., 2015a). Using a 3-way automated magnetic dual switching unit (Tekran® Model 1110), the DFC inlet and outlet gas were sequentially sampled into the Hg vapor analyzer at 10-min intervals (two 5-min samples, flow rate = 1.0 L min^{-1}). Hg^0 flux was calculated according to:

$$F = \frac{Q \cdot (C_{out} - C_{in})}{A} \quad (1)$$

where F is Hg^0 flux (ng m^{-2} h^{-1}), A is the DFC footprint (0.06 m^2), Q

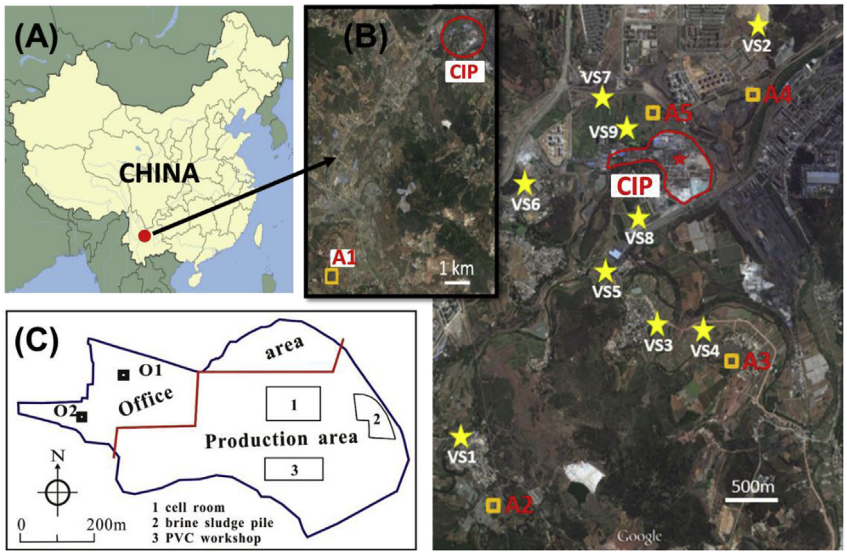

Fig. 1. Map showing: (A) the location of the CIP, (B) ambient Hg^0 concentration, surface soils and air-soil Hg^0 flux sampling sites surrounding the CIP, (C) spatial distribution of the Hg^0 measurement sites at the vicinity of the CIP.

is the flushing flow rate (0.9 $m^3\ h^{-1}$), C_{out} and C_{in} are the Hg^0 concentrations of the DFC outlet and inlet gas samples, respectively. A positive sign *F* represents emission and a negative sign *F* indicates deposition. Considering that a long DFC turnover time (TOT) may lead to an underestimation of Hg flux (Eckley et al., 2010; Lin et al., 2012; Lindberg et al., 2002), a constant and relatively high flow rate (15 L min^{-1}, TOT = 0.32 min) was applied in consistence with previous studies (Feng et al., 2005; Fu et al., 2012; Fu et al., 2008; Wang et al., 2006; Zhu et al., 2011; Zhu et al., 2015a; b). A quartz tube filled with dry soda-lime was assembled in front of the instrument gas inlet to remove particles and acidic gases. Tekran® 2537B was calibrated before the field campaign using manual injections of a known amount of Hg^0 vapor yielding a recovery of 97%–101% (n = 4 for each of the two gold traps). In the field, the instrument was manually calibrated using an internal Hg^0 permeation source before and after the sampling at each site. Prior to the field campaign, the DFC was cleaned by 10% nitric acid followed by ultrapure water (18.2 MΩ cm, Millipore Corp.). The DFC blank (0.4 ± 0.7 ng $m^{-2}\ h^{-1}$, n = 14) was found to be low and not corrected for in the reported flux (Eq. (1)). After Hg^0 flux sampling, the surface soils (~2 cm) covered in DFC footprint was collected for subsequent total Hg content (THg) and Hg isotope ratios analysis in the laboratory.

Parallel to Hg^0 flux measurement, synchronized 5-min averaged meteorological data including solar radiation, air temperature, soil temperature, wind speed, wind direction, relative humidity, and soil moisture were recorded at each sampling site using a portable weather station (HOBO U-30, Onset Corp., USA).

2.3. Measurement of soil pore gas Hg^0 concentration

A 5-L cylindrical Teflon flask (20 cm height), with 2 mm diameter holes uniformly distributed (10 mm distance between hole centers) over its buried surface, was applied for measuring Hg^0 concentration in soil pore gas (Fu et al., 2012). At each of the five flux sampling sites, the Teflon flask was rammed into the soil manually and allowed to equilibrate in the soil for ~12 h before the sampling was initiated. The soil pore gas was continuously extracted from the outlet of the Teflon flask at a low flow rate of 0.2 L min^{-1} using the 2537B instrument. The soil gas Hg^0 was concentrated for 10 min on its internal gold cartridges and then desorbed and analyzed. The measured soil gas Hg^0 concentration was relatively stable over time and found not discernibly correlated with concentration fluctuations in ambient air, indicating air intrusion into the soil was insignificant. It should, however, be noted that the measured soil pore gas Hg^0 in this study represented a mixed Hg^0 pool down to a depth of ~20 cm.

2.4. Measurement of soil total Hg concentration and Hg isotope ratios

The surface soil samples (upper ~2 cm) at the five flux sampling sites (A1-A5) were collected, stored in clean polyethylene bags and transported to the lab together with soils collected at the other 9 sites (0–2 cm, VS1–VS9, Fig. 1B) representing various land use and distances to the CIP. All soil samples were freeze-dried in the lab, milled and sieved through 100 mesh, and stored in clean bags until analysis. Soil THg was determined using a Lumex® RA-915 + Hg vapor analyzer coupled with a PYRO 915 + pyrolysis atomizer (Zhu et al., 2013a). Triplicated measurement of soil samples showed 96%–104% reproducibility. A certified soil material (GSS-5, Institute of Geophysics and Geochemical Exploration, China) was used for QA/QC. The measured THg concentration of GSS-5 (298.1 ± 11.7 ng g^{-1}, n = 5) was within the specification of the certified value of 290 ± 30 ng g^{-1}.

To extract soil THg for Hg isotope ratio analysis, soil samples (~0.2–0.5 g) were weighed and digested in 5 ml of freshly prepared aqua regia (HNO_3:HCl = 1:3, v/v, high purity grade) kept at > 95 °C in a water bath. Hg isotopes were measured by CV-MC-ICP-MS (Nu Plasma, Nu Instruments, UK) following a well-established methodology using sample-standard bracketing (SRM 3133, NIST, USA) and Tl (SRM 997) addition for mass bias correction (Yin et al., 2010). Digested sample and reduction reagent ($SnCl_2$ solution) were mixed online by a custom-made continuous flow cold-vapor generation and liquid-gas separation system (Lin et al., 2015). Before analysis, a digested sample was diluted to a concentration of ~1 ng Hg ml^{-1} in ~10% aqua regia for analytical consistency. The bracketing NIST SRM-3133 standards were prepared to closely match the Hg concentration (<10% variability) and acid content of the analyzed samples (Yu et al., 2016). The instrument was set to

acquire data twice for Hg masses (198, 199, 200, 201 and 202) and Tl masses (203 and 205) for one block (100 cycles and 6 s integration time per cycle). In parallel, UM-Almadén was analyzed regularly as a secondary standard. Hg isotope ratios are reported in delta notation (δ^{xxx}Hg, ‰) relative to the standard NIST SRM 3133:

$$\delta^{xxx}\mathrm{Hg} = \left[\frac{(^{xxx}\mathrm{Hg}/^{198}\mathrm{Hg})_{\mathrm{sample}}}{(^{xxx}\mathrm{Hg}/^{198}\mathrm{Hg})_{\mathrm{SRM3133}}}\right] \times 1000 \quad (2)$$

where *xxx* indicates the mass of isotopes 199, 200, 201, 202, and 204. δ^{202}Hg was used as the basis to assess mass-dependent fractionation (MDF). In turn, mass-independent fractionation (MIF) is calculated as follows (Bergquist and Blum, 2007):

$$\Delta^{199}\mathrm{Hg} = \delta^{199}\mathrm{Hg} - \left(\delta^{202}\mathrm{Hg} \times 0.2520\right) \quad (3)$$

$$\Delta^{200}\mathrm{Hg} = \delta^{200}\mathrm{Hg} - \left(\delta^{202}\mathrm{Hg} \times 0.5024\right) \quad (4)$$

$$\Delta^{201}\mathrm{Hg} = \delta^{201}\mathrm{Hg} - \left(\delta^{202}\mathrm{Hg} \times 0.7520\right) \quad (5)$$

The measured isotope ratios of UM-Almadén (δ^{202}Hg = −0.53 ± 0.12‰, Δ^{199}Hg = −0.02 ± 0.09‰, Δ^{200}Hg = 0.01 ± 0.04‰, Δ^{201}Hg = 0.04 ± 0.07‰, 2SD, n = 7) was in agreement with literature data (Blum and Bergquist, 2007) and measurements in our lab (Liu et al., 2011; Yin et al., 2015; Yin et al., 2013; Yin et al., 2010; Yu et al., 2016). It should be noted the reported individual sample isotopic ratio uncertainty representing the larger standard deviation (2SD) of either duplicate analyzed single soil digest or UM-Almadén measurement reproducibility in the whole session (Blum and Bergquist, 2007).

3. Results and discussion

3.1. Spatial distribution of soil THg and ambient Hg^0 concentrations

The THg concentrations in soils from 14 sampling locations with various distances to CIP are presented in Tables 1 and 2. Overall, soil THg displays an increasing trend from the most distant site A1 at 11.5 km towards the CIP area (Table 2). Hg concentration in soils near the CIP is up to 2 orders of magnitude higher than the local background, reflected in the concentration range from 67 ng g^{-1} at 11.5 km to 4790 ng g^{-1} outside of the cell house (0.4 km). The spatial trend in soil THg with distance is approximated with an exponential decay fit of [THg] = 3631·exp(-1.5·*d*) + 176 (r = 0.64, p = 0.06, n = 14), where *d* and [THg] represent the distance (*km*) from the CIP Hg-cell house and soil THg concentration (ng g^{-1}), respectively. Similar trends have been observed near CAPs and other anthropogenic point sources (e.g., Pb/Zn smelters), which is linked to the cumulative deposition of emitted Hg (Estrade et al., 2011; Grangeon et al., 2012; Li et al., 2013; Li et al., 2011). The capacity of soils to retain deposited Hg over time is controlled by a multitude of soil factors (e.g., organic matter, moisture, alkalinity) (Biester et al., 2002; Cachada et al., 2009; Hissler and Probst, 2006; Sommar et al., 2016). In this study, a substantial variation of up to 2.3 times of magnitude in soil THg concentration was observed for the approximately equidistant sites A4, VS3 and VS4 from the CIP. Meanwhile, higher Hg was accumulated in the organic grove soil (VS2) than the bare soil (VS4), although VS4 was closer to the point source.

After the closure of the point Hg source, the near-ground atmospheric Hg^0 concentration from A1 to A5 gradually increase from distant site (A1) towards the abandoned CIP. The diel mean

Table 1
Statistical summary of air-soil Hg^0 fluxes, air Hg^0 concentration, Hg contents in soils and averaged meteorological parameters in the field measurements.

Sites	Distance (km)	Hg^0 flux (ng m^{-2} h^{-1})						Hg^0 concentration (ng m^{-3})			Soil THg (ng g^{-1})	Meteorological parameter				
		Mean	Std	Range	N (Emission)	Day mean	Night mean	Mean	Std	Range		Solar radiation (W m^{-2})	Air Humi (%)	Soil temp (°C)	Wind speed (m s^{-1})	Wind direction (°)
A1	11.5	15.1	28.2	−11.9–85.4	72(46)	31.7	−0.7	3.3	0.5	2.5–4.6	67	206	55.9	15.9	2.48	88.5
A2	6.5	26.9	43.5	−28.7–193.3	72(48)	52.2	1.7	4.2	0.7	3.3–6.1	153	243	66.1	18.0	4.47	175.5
A3	3.2	56.4	58.3	−0.8–219.4	72(71)	95.1	17.6	4.8	1.9	3.2–10.8	240	218	53.0	17.2	2.65	205.4
A4	1.8	64.2	82.1	−23.6–345.0	72(56)	119.6	8.7	6.9	2.4	3.7–11.9	307	190	66.7	16.8	1.20	106.5
A5	0.75	348.2	364.5	−141.2–1052.0	72(65)	620.4	55.4	10.5	2.8	6.1–19.8	686	203	68.9	18.1	1.54	98.9

Table 2
Total Hg concentration and isotope signatures of surface soils in the vicinity of the closed industrial plant, and UM-Almadén reference (AMD, n = 7). The 2σ represented the measurement reproducibility of single soil digest and the UM-Almadén standard.

Samples ID	Distance km	THg (ng g^{-1})	δ^{202}Hg ‰	2σ ‰	Δ^{199}Hg ‰	2σ ‰	Δ^{200}Hg ‰	2σ ‰	Δ^{201}Hg ‰	2σ ‰	Classification
A1	11.5	67	−2.11	0.12	−0.05	0.05	0.00	0.05	−0.06	0.07	Agricultural land
A2	6.5	153	−1.92	0.12	−0.22	0.05	−0.01	0.05	−0.22	0.07	Agricultural land
A3	3.2	240	−1.73	0.12	−0.06	0.05	−0.04	0.05	−0.11	0.07	Agricultural land
A4	1.8	307	−1.49	0.12	0.01	0.05	−0.02	0.04	−0.03	0.07	Agricultural land
A5	0.75	686	−0.40	0.12	−0.07	0.05	0.00	0.04	−0.09	0.07	Agricultural land
VS1	6.2	163	−1.74	0.12	−0.12	0.05	0.01	0.04	−0.12	0.07	Grove soil
VS2	1.9	660	−0.75	0.12	−0.07	0.05	−0.01	0.04	−0.09	0.07	Grove soil
VS3	1.4	720	−1.04	0.12	−0.07	0.05	−0.02	0.04	−0.07	0.07	Agricultural land
VS4	1.4	437	−1.07	0.12	−0.04	0.05	−0.04	0.04	−0.04	0.07	Bare soil
VS5	1.1	1304	−0.39	0.12	−0.09	0.05	0.08	0.04	−0.09	0.07	Agricultural land
VS6	1.0	980	−0.07	0.12	−0.11	0.09	0.01	0.04	−0.11	0.07	Orchard
VS7	0.6	552	−0.88	0.12	−0.02	0.05	0.00	0.04	−0.04	0.07	Wet paddy
VS8	0.4	4790	0.11	0.12	−0.03	0.05	0.00	0.04	−0.02	0.07	Grassland
VS9	0.3	1070	0.72	0.12	0.00	0.05	0.01	0.04	0.01	0.07	Agricultural land
AMD			−0.53	0.12	−0.02	0.05	0.01	0.04	−0.04	0.07	

ambient Hg^0 increased from 3.3 ng m^{-3} at A1 (11.5 km) to 10.5 ng m^{-3} at A5 (0.75 km) (Table 1 and Fig. 2, $p < 0.001$ for mean values between all five sites, one-way ANOVA post hoc Turkey multiple comparison), which corresponds to the soil THg contents (Fig. 2B). Ambient Hg^0 concentration at the farthest 11.5 km away from the CIP of 3.3 ng m^{-3} was over 50% magnitude higher than the regional background concentration (Ailao Mt., ~2.1 ± 0.6 ng m^{-3}) (Zhang et al., 2016a). O1 and O2 located in the west of the CIP, with a similar distance from A5 to the closed Hg-cell-room, have a comparably elevated ambient Hg^0 concentration (Fig. 2A). Meanwhile, measurements of ambient air Hg^0 inside and outside the CAP Hg-cell room (mean: 212 and 35.4 ng m^{-3}, respectively) and PVC workshop (2668 and 188 ng m^{-3}), near-ground air above brine-sludge waste pile (620 ng m^{-3}) exhibited highly elevated Hg^0 concentration, at 1–3 orders magnitude higher than the values measured in natural areas immediately outside the CIP (e.g., A5, ≤10 ng m^{-3}). This suggests that the CIP site remained a strong Hg^0 emission source. There is a lack of data documenting Hg^0 pollution during active operation of CAP in China, yet Southworth et al. (2004) reported a 2–3 orders magnitude elevated gaseous Hg^0 in the cell room (130 ± 20 μg m^{-3}) and at a distance of 500 m (100–1000 ng m^{-3}) from an active CAP in the US. The average air Hg^0 concentrations at PI (2.7 μg m^{-3}) and PO (0.2 μg m^{-3}) were much lower than an operated PVC workshop located in Central China of 10–15 and 5 μg m^{-3}, correspondingly (Ren et al., 2014).

The highly elevated Hg^0 concentration in the CIP and the concentration gradient of air Hg^0 demonstrate that the closed facility remained a Hg emission/diffusion source. The source caused events of elevated ambient Hg^0 during nighttime at site A5, yielding ambient Hg^0 concentration up to 20 ng m^{-3} accompanied with a low air-soil Hg^0 flux. The strongly positive correlation between ambient Hg^0 and soil THg concentration and soil-air Hg^0 flux (Fig. 2B) suggests that the re-emission of the deposited Hg accumulated over time also contributed to the elevated atmospheric Hg measured in the area surrounding the CIP (c.f. discussion in 3.3).

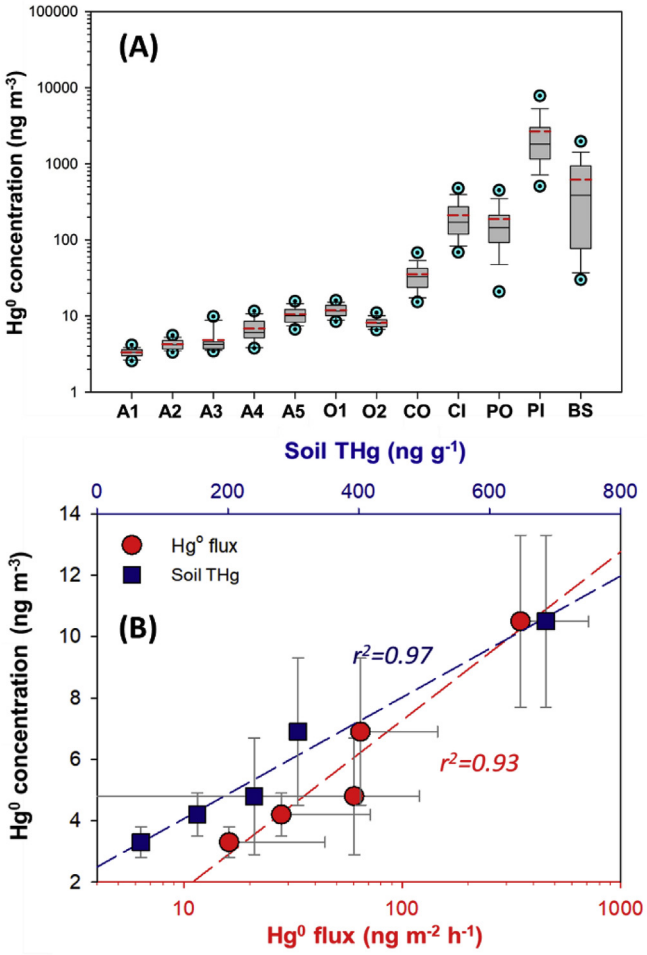

Fig. 2. (A) Box and whisker plot of Hg^0 concentration observed at the sites at the vicinity of and within the CIP. The two box horizontal border line represent 25th and 75th percentiles, the whisker indicate 10th and 90th percentiles, and the outliers indicate 5th and 95th percentiles. Solid black line and bold red dash line in the box indicate median and mean. A1 to A5 represent the five vicinity natural soil surfaces, O1 and O2 represent two sites located in the administrative-office area of industrial plant (cf. Fig. 1c), CO and CI represent the outdoor and indoor of the closed Hg-cell room, PO and PI represent the outdoor and indoor of closed PVC workshop, and BS represents measurement above the brine sludge waste pile. (B) The relationship between ambient air Hg^0 concentration and the surface soil THg concentration, *in-situ* daily averaged (±SD) Hg^0 flux. (For interpretation of the references to colour in this figure legend, the reader is referred to the Web version of this article.)

3.2. Historic sources of THg recorded in contaminated soil

The isotope compositions of soil Hg in the surface soil samples collected during the campaign are presented in Table 2. The MDF varied in a large range ($\delta^{202}Hg = -2.11‰$ to 0.72‰) and displayed an increasing enrichment in heavier isotopes from background (lower THg) to contaminated soil (Higher THg). The soil samples displayed a narrow range of near-zero MIF ($\Delta^{199}Hg = = -0.07 \pm 0.06‰$, 1SD; $\Delta^{200}Hg = 0.00‰ \pm 0.03‰$, 1SD; n = 14).

Multiple processes including Hg(II) reduction and leaching have been reported to cause MDF and MIF of Hg isotopes in different environmental media (Jiskra et al., 2015; Washburn et al., 2017; Yin et al., 2013, 2015). Reduction of Hg(II) through photo and dark pathways mediated by organic matter leads to substantial MIF (Bergquist and Blum, 2007; Zheng and Hintelmann, 2010). Only three soil samples (A2, VS1 and VS6) displayed significant negative MIF ($\Delta^{199}Hg \leq -0.10‰$) in this study. Substantial Hg^0 emission flux from soil near CIP was observed (Table 1). The observed Hg^0 flux was highly correlated with solar radiation (section 3.3), implying light induced Hg(II) photochemical processes (e.g., photoreduction or reduction triggered by photochemically formed reactive intermediates) played an important role. The $\Delta^{199}Hg/\Delta^{201}Hg$ ratio exhibited a slope of 0.969, consistent with magnetic isotope effect induced fractionation during Hg(II) photoreduction (Bergquist and Blum, 2007). However, both ^{199}Hg and ^{202}Hg would be progressively enriched in soil as the photochemically driven Hg^0 evasion proceeds. Therefore, the negative MIF signals should be inherited from Hg sources prior to deposition. Previous studies have documented that surface soil can preserve the isotopic fingerprints of Hg sources (Estrade et al., 2011; Feng et al., 2013; Zhang et al., 2013). The sporadic observed MIF variation was likely stemmed from additional contribution such as background atmospheric Hg^0. The regional background atmospheric Hg^0 pool was reported as $\delta^{202}Hg = 0.52 \pm 0.30‰$ and $\Delta^{199}Hg = -0.18 \pm 0.03‰$, whilst corresponded litterfall constituted $\delta^{202}Hg = -3.03 \pm 0.28‰$ and $\Delta^{199}Hg = -0.40 \pm 0.08‰$ (Yu et al., 2016), in line with the observed MIF value at low THg site A2. Soil samples from A2, VS1 and VS6 are located in agricultural, grove and orchard lands with substantial vegetative biomass production. Uptake of atmospheric Hg^0 by vegetation could have contributed to the observed negative MIF in the soil samples.

Fig. 3 shows the MDF in soil THg ($\delta^{202}Hg$) against 1/[THg]. An inverse linear relationship ($r^2 = 0.72$) was obtained except for the samples collected at A1, A2 and VS1, suggesting that Hg isotopic composition was caused by the binary mixing of two distinct sources (Foucher et al., 2009). The Hg pollution source from the CIP operation can be characterized as $\delta^{202}Hg = 0.27‰$ (1/[THg] → 0). It

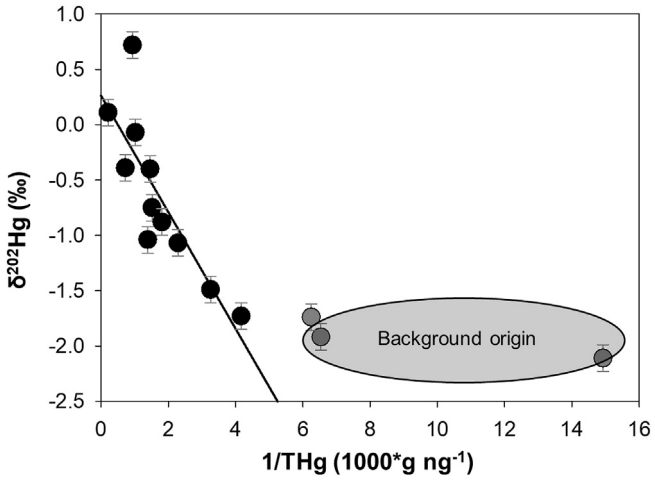

Fig. 3. Plots and correlation between mass dependent fractionation ($\delta^{202}Hg \pm 2SD$) of Hg in natural vicinity surface soils and 1/[THg].

should be noted that the $\delta^{202}Hg$ endmember representing industrial Hg source may consist of multiple sources in the CIP (liquid Hg used in the CAP and Hg(II) used in the PVC sector). Subsequent fractionation caused by volatilization and deposition processes potentially altered the initial source signature during transport to the surface soils. Despite THg concentration in A1, A2 and VS1 varied by a factor of 3, the THg isotopic composition did not show significant variation and thus can be assigned as the regional background source signatures ($\delta^{202}Hg = -1.92 \pm 0.18‰$, $n = 3$, $6 < 1/[THg] < 16$). Slight scatter along the regression was observed, for example, $\delta^{202}Hg$ of VS9 was significantly higher than the linear relationship projected industrial source isotopic signature. VS9 was the closest to the CIP where other sources such as surface runoff might also be of contribution, which was distinct from predominant atmospheric originated deposition of Hg at other sites, and therefore this sample is not relevant to decide the binary source mixing. The binary isotope mass balance model estimating the relative sources contribution can be expressed as:

$$X_{cont}\delta^{202}Hg_{cont} + X_{nat}\delta^{202}Hg_{nat} = \delta^{202}Hg_{soils} \quad (6)$$

$$X_{cont} + X_{nat} = 1 \quad (7)$$

where X_{cont} and X_{nat} are the fractions of Hg originated from industrial contaminant and regional background sources, respectively. $\delta^{202}Hg_{cont}$ and $\delta^{202}Hg_{nat}$ are above discussed two endmembers.

The modeled sources contribution along the distance away from the CIP were presented in Fig. 4. As expected, Hg input from the industry plant to soil decreased with the increasing distance from the CIP and was predominant within a 6.5-km radius. Soil samples collected outside (e.g., A1 and A2) show a strong influence by background sources. Within 2 km, the dominant source in soil was caused by the industry plant, as evidenced by the VS8 and VS9 data (>95% is of industrial source origin).

3.3. Hg^0 flux from soil in the vicinity of the closed industry plant

The daily average Hg^0 flux from the background agricultural soil (i.e., A1 and A2) ranged from 15.1 to 26.9 ng m^{-2} h^{-1} during the dry spring season (Table 1). The Hg^0 flux is comparable with observations at agricultural sites in Chongqing (46.5 ± 22.8 ng m^{-2} h^{-1}) and Guizhou (16.5 ng m^{-2} h^{-1}) in Southwest China (Feng et al., 2005; Zhu et al., 2011). However, Hg^0 flux was progressively increased from A3, A4, to more than one order of magnitude higher at A5 (348.2 ng m^{-2} h^{-1}), corresponding to the gradually increased soil Hg caused by the industry plant pollution.

Previous studies have shown that soil Hg contents control Hg^0 evasion under comparable meteorological conditions (e.g., solar radiation and soil temperature) (Feng et al., 2005; Gustin et al., 1999; Lin et al., 2010; Wang et al., 2005). The measured Hg^0 flux

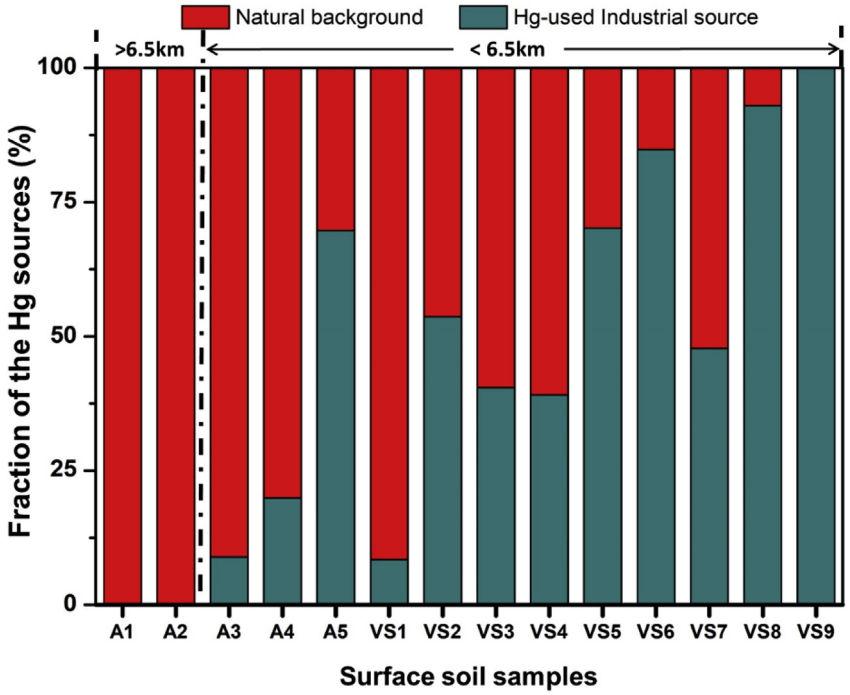

Fig. 4. Binary Hg isotope model estimated fractions of chlor-alkali industry and regional background Hg sources contribution in surface soils at the vicinity of the CIP.

from soil exhibited a similar diurnal feature, with significantly higher evasion during daytime and lower flux at nighttime (Fig. 5). The daytime flux was correlated with solar radiation ($r^2 = 0.77–0.91$, $p < 0.001$) and soil temperature ($r^2 = 0.60–0.92$, $p < 0.001$), indicating the role of photoreduction (Gustin et al., 2002) and the enhanced evasion driven by higher temperature (Lin et al., 2010). At the background sites A1 and A2, the nighttime flux was near zero and remained relatively stable over time, in agreement with nighttime flux measured elsewhere (Zhu et al., 2016). Significant nighttime evasion was observed at the polluted sites A3, A4 and A5, possibly caused by the intensive daytime photo-reduction that formed Hg^0, which was continuously desorbed and released from soil (Eckley et al., 2015). The observed Hg^0 in soil pore gas was also elevated at these industrial polluted sites (A3, A4 and A5) compared to the regional background sites (A1 and A2) ($p < 0.001$, one-way ANOVA, Fig. 6). This indicates that the contaminated soil is likely associated with higher concentrations of loosely-bound soil Hg^0, corresponding well with the overall higher average diel Hg^0 flux. In contrast to the vertical depletion of soil gas Hg^0 versus atmospheric Hg^0 measured in two US forests in the Sierra Nevada mountains (Obrist et al., 2014), the consistently higher levels of soil pore gas Hg^0 relative to near-ground ambient Hg^0 suggests that the soil column (down to ~20 cm) represents a diffusive source of Hg^0 to the atmosphere. However, the soil pore gas Hg^0 was not simply depended on the soil Hg content, as indicated by the statistically similar values observed at the sites within both polluted (A3, A4 and A5) and background (A1 and A2) groups.

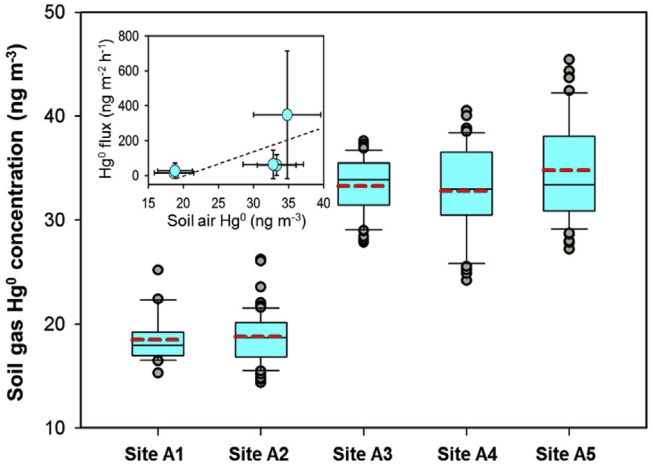

Fig. 6. Box and whisker plot of soil pore-gas Hg^0 concentrations at the flux sampling sites. Two box horizontal border lines indicate 25th and 75th percentiles, whisker indicate 10th and 90th percentiles, and circles indicate outliers. Solid black line and red short line in the box indicate median and mean concentration. Inlaid is a plot of soil pore-gas Hg^0 concentrations versus average diel Hg^0 flux (error bar denotes ±SD). (For interpretation of the references to colour in this figure legend, the reader is referred to the Web version of this article.)

Factors such as redox potential, temperature, organic matter, etc., could have also influenced the measured Hg^0 concentrations in soil pore gas (Moore and Castro, 2012).

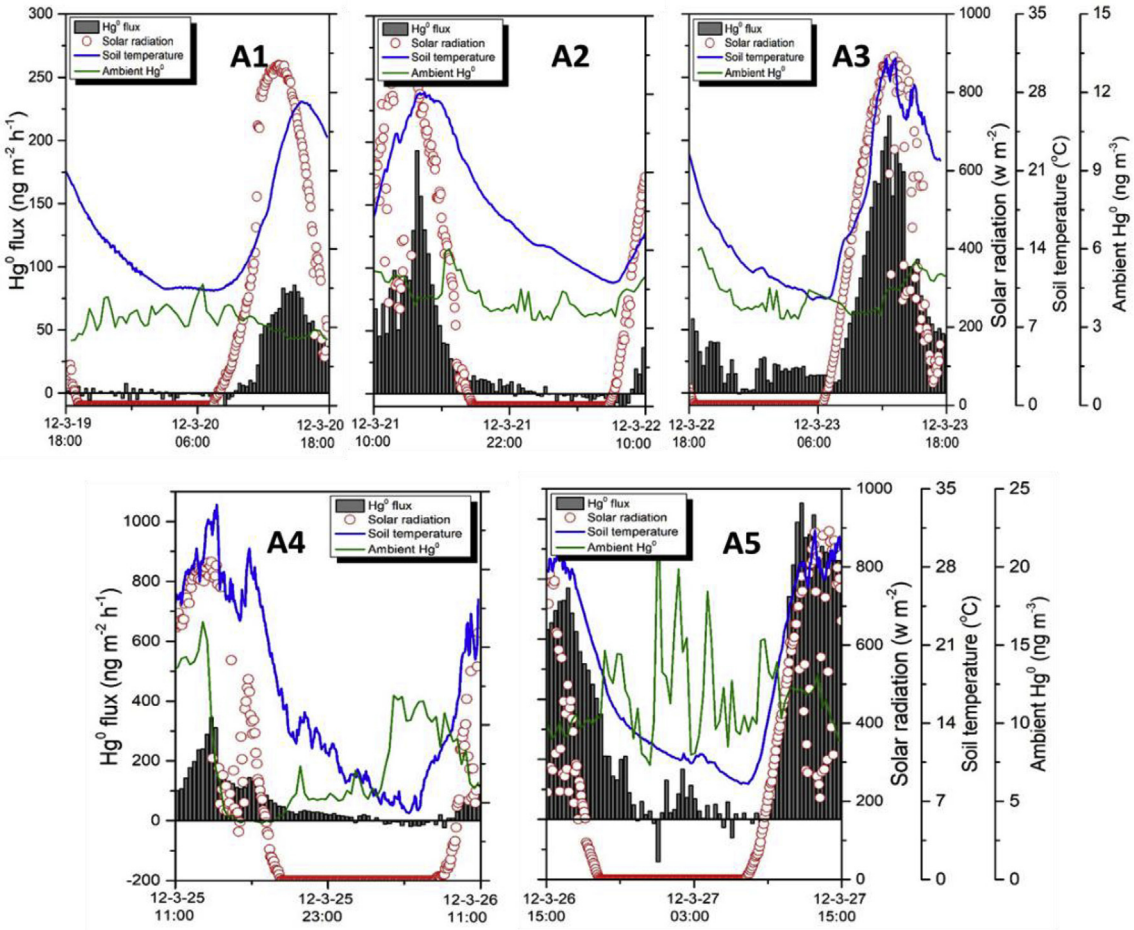

Fig. 5. Diurnal patterns of Hg^0 fluxes, solar radiation, soil temperature and near-ground ambient Hg^0 from the vicinity agricultural soil surfaces (Note the difference in Y-axis scales of Hg^0 flux and ambient Hg^0 concentration for upper and lower panels).

The air Hg^0 concentration near soil surface displayed a significant correlation with the averaged Hg^0 flux and soil Hg content (Fig. 2B), consistent with the observation at a closed point Hg source in Canada (Eckley et al., 2013). However, we did not observe a significant correlation between instantaneous Hg^0 flux and Hg^0 concentration at all sites. The daytime ambient Hg^0 at the polluted sites A3 and A4 was higher than the nighttime Hg^0 concentration, whereas substantially higher Hg^0 was observed during nighttime at a relatively nearby site A5 (Fig. 5). It is known that ambient Hg^0 concentration suppressing Hg^0 flux, as reflected by the large deposition event at site A5 (-141.2 ng m^{-2} h^{-1}). This suggests that the re-emitted Hg^0 could have contributed to the near-ground Hg^0 concentration at A3 and A4, while the atmospheric transport of Hg^0 from the CIP controlled the Hg^0 concentration at A5.

3.4. Evidence of reemission of legacy Hg deposition

During the 5-decade of active operation, the wet and dry deposition of Hg enhanced by the industry plant to the surrounding area greatly increased soil THg concentration [from $\leq$150 to 4790 ng g^{-1}]. Although the rainwater and ambient gaseous/particulate Hg(II) concentration was not available when the plant was in operation, previous studies have showed that closure of point Hg emission source effectively reduces Hg(II) wet and dry deposition by a factor of 3 to an order of magnitude for Pb/Zn smelters and coal-power plants (Eckley et al., 2013; Rothenberg et al., 2010). The elevated ambient Hg^0 concentration caused by the immediate emissions during operation of the point Hg source suppressed air-surface Hg^0 exchange resulted in net deposition of Hg^0 and soil contamination (Eckley et al., 2015). Similar processes should also occur at this site for 5 decades. Therefore, after the closure the CAP and PVC production activities, a strong net reemission of previously deposited Hg into the atmosphere was evident.

Hg^0 efflux typically increases with increasing soil Hg content, either linearly (Lin et al., 2010) or exponentially (Agnan et al., 2016). Given the available data observed in this study, the daily average Hg^0 flux is linearly correlated to industrial-originated Hg content (as estimated in Fig. 4). Fig. 7 shows the correlation between soil Hg from industrial sources and the average Hg^0 flux measured at the site. The intercept of the regression analysis suggests an average background emission of Hg^0 at $\leq$ 30 ng m^{-2} h^{-1}. The daily average Hg^0 reemission rate contributed by the industrial plant was estimated to be 0.63[Hg_{cont}] ng m^{-2} h^{-1} (Fig. 7). Using the regression relationship (Hg^0 flux = 0.63[Hg_{cont}] + 29.9), Hg^0 flux contributed by the industrial sources outside the CIP was estimated. The daily mean Hg^0 re-emission flux calculated as the difference between the model-estimated background flux and the observed flux was up to ~2700 ng m^{-2} h^{-1} at site VS8 of highest soil THg. Although significant uncertainty may exist in the estimate due to limited data in establishing the correlation coefficient, the magnitude of reemission flux over soil was as large as those measured over geologically enriched mines (Eckley et al., 2011; Gustin et al., 2003; Wang et al., 2005; Zhu et al., 2016). This suggests that the natural surfaces surrounding a closed facility can be activated as a strong diffused nonpoint source of Hg^0 emission similar to those found over typical Hg enriched mine surfaces.

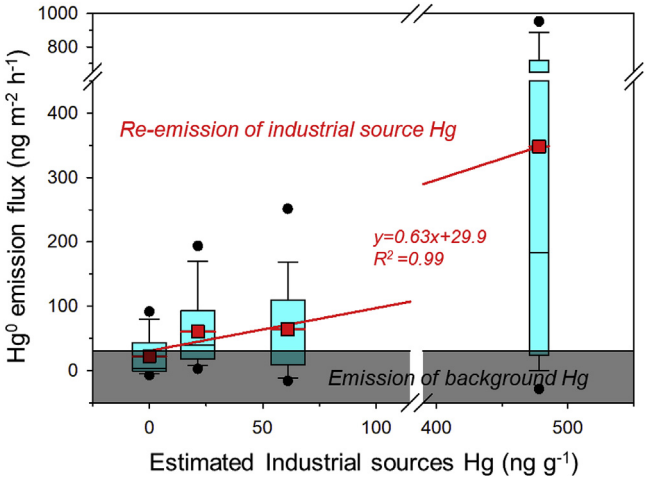

Fig. 7. Relationship between observed Hg^0 flux and estimated industrial source Hg in soils. Shaded area represents the estimated Hg^0 emission from regional background source Hg, the upper parts represents reemission of Hg originated from the industrial source.

4. Conclusions and implications

Through comprehensive observation of *in-situ* Hg^0 flux, THg concentration and stable Hg isotope ratios analysis, it has been found that the CAP/PVC facility after closure sill represented a strong emission source from the Hg-containing wastes and previously deposited Hg. Hg released from the plant was gradually accumulated in the natural area surrounding the closed industrial facilities (up to 6.5-km radius range). After closure, the plant and its remaining Hg wastes (i.e., electrolysis sludge and Hg-catalyst waste) still represent strong sources releasing Hg to the surrounding natural area. Meanwhile, the nearby 6.5-km natural soils reemit the previous deposited legacy Hg to the atmosphere with a magnitude as large as geological enriched surfaces.

Reducing Hg emission from large point sources by improving the technology or closing the source is expected as required by the Minamata Convention. For example, China has replaced high-Hg catalyst with low-Hg catalyst technology and implemented effective Hg emission reduction in the PVC industry (Lin et al., 2016). The continued Hg^0 emission from legacy Hg deposition caused by the closed industrial facilities could be overlooked and requires attention. It is therefore important that future studies on Hg inventory devote attention to natural surfaces surrounding contaminated sites since its Hg evasion flux can be up to 2–3 orders of magnitude higher than the background soil surfaces after the closure of point sources.

Acknowledgements

This research was financially supported by National Science Foundation of China (grants 41503122, 41373056, 41430754 and 21661132002) and by K.C.Wong Education Foundation.

References

Agnan, Y., Le Dantec, T., Moore, C.W., Edwards, G.C., Obrist, D., 2016. New constraints on terrestrial surface–atmosphere fluxes of gaseous elemental mercury using a global database. Environ. Sci. Technol. 50, 507–524.
AMAP/UNEP, 2013. Technical Background Report for the Global Mercury Assessment 2013. Arctic Monitoring and Assessment Programme, Oslo, Norway/UNEP Chemicals Branch, Geneva, Switzerland, p. 263.
Amos, H.M., Sonke, J.E., Obrist, D., Robins, N., Hagan, N., Horowitz, H.M., Mason, R.P., Witt, M., Hedgecock, I.M., Corbitt, E.S., Sunderland, E.M., 2015. Observational and modeling constraints on global anthropogenic enrichment of mercury. Environ. Sci. Technol. 49, 4036–4047.
Bergquist, B.A., Blum, J.D., 2007. Mass-dependent and -independent fractionation of Hg isotopes by photoreduction in aquatic systems. Science 318, 417–420.
Biester, H., Müller, G., Schöler, H.F., 2002. Estimating distribution and retention of mercury in three different soils contaminated by emissions from chlor-alkali plants: part I. Sci. Total Environ. 284, 177–189.
Blum, J.D., Bergquist, B.A., 2007. Reporting of variations in the natural isotopic composition of mercury. Anal. Bioanal. Chem. 388, 353–359.
Cachada, A., Rodrigues, S.M., Mieiro, C., Ferreira da Silva, E., Pereira, E., Duarte, A.C.,

2009. Controlling factors and environmental implications of mercury contamination in urban and agricultural soils under a long-term influence of a chlor-alkali plant in the North–West Portugal. Environ. Geol. 57, 91–98.
Carpi, A., Lindberg, S.E., 1997. Sunlight-mediated emission of elemental mercury from soil amended with municipal sewage sludge. Environ. Sci. Technol. 31, 2085–2091.
Eckley, C.S., Blanchard, P., McLennan, D., Mintz, R., Sekela, M., 2015. Soil–air mercury flux near a large industrial emission source before and after closure (Flin Flon, Manitoba, Canada). Environ. Sci. Technol. 49, 9750–9757.
Eckley, C.S., Gustin, M., Lin, C.J., Li, X., Miller, M.B., 2010. The influence of dynamic chamber design and operating parameters on calculated surface-to-air mercury fluxes. Atmos. Environ. 44, 194–203.
Eckley, C.S., Gustin, M., Marsik, F., Miller, M.B., 2011. Measurement of surface mercury fluxes at active industrial gold mines in Nevada (USA). Sci. Total Environ. 409, 514–522.
Eckley, C.S., Parsons, M.T., Mintz, R., Lapalme, M., Mazur, M., Tordon, R., Elleman, R., Graydon, J.A., Blanchard, P., St. Louis, V., 2013. Impact of closing Canada's largest point-source of mercury emissions on local atmospheric mercury concentrations. Environ. Sci. Technol. 47, 10339–10348.
Estrade, N., Carignan, J., Donard, O.F.X., 2011. Tracing and quantifying anthropogenic mercury sources in soils of northern France using isotopic signatures. Environ. Sci. Technol. 45, 1235–1242.
Feng, X., Yin, R., Yu, B., Du, B., 2013. Mercury isotope variations in surface soils in different contaminated areas in Guizhou Province, China. Chin. Sci. Bull. 58, 249–255.
Feng, X.B., Wang, S.F., Qiu, G.L., Hou, Y.M., Tang, S.L., 2005. Total gaseous mercury emissions from soil in Guiyang, Guizhou, China. J. Geophys. Res. Atmos. 110, D14306.
Foucher, D., Ogrinc, N., Hintelmann, H., 2009. Tracing mercury contamination from the idrija mining region (Slovenia) to the gulf of trieste using Hg isotope ratio measurements. Environ. Sci. Technol. 43, 33–39.
Fritsche, J., Obrist, D., Alewell, C., 2008. Evidence of microbial control of Hg^0 emissions from uncontaminated terrestrial soils. J. Plant Nutr. Soil Sci. 171, 200–209.
Fu, X., Feng, X., Zhang, H., Yu, B., Chen, L., 2012. Mercury emissions from natural surfaces highly impacted by human activities in Guangzhou Province, South China. Atmos. Environ. 54, 185–193.
Fu, X.W., Feng, X.B., Zhu, W.Z., Wang, S.F., Lu, J.L., 2008. Total gaseous mercury concentrations in ambient air in the eastern slope of Mt. Gongga, South-Eastern fringe of the Tibetan plateau, China. Atmos. Environ. 42, 970–979.
Grangeon, S., Guedron, S., Asta, J., Sarret, G., Charlet, L., 2012. Lichen and soil as indicators of an atmospheric mercury contamination in the vicinity of a chlor-alkali plant (Grenoble, France). Ecol. Indicat. 13, 178–183.
Grönlund, R., Sjoholm, M., Weibring, P., Edner, H., Svanberg, S., 2005. Elemental mercury emissions from chlor-alkali plants measured by lidar techniques. Atmos. Environ. 39, 7474–7480.
Gustin, M.S., 2011. Exchange of mercury between the atmosphere and terrestrial ecosystems. In: Liu, G.L., Cai, Y., O'Driscoll, N. (Eds.), Environmental Chemistry and Toxicology of Mercury, pp. 423–451.
Gustin, M.S., Biester, H., Kim, C.S., 2002. Investigation of the light-enhanced emission of mercury from naturally enriched substrates. Atmos. Environ. 36, 3241–3254.
Gustin, M.S., Coolbaugh, M.F., Engle, M.A., Fitzgerald, B.C., Keislar, R.E., Lindberg, S.E., Nacht, D.M., Quashnick, J., Rytuba, J.J., Sladek, C., Zhang, H., Zehner, R.E., 2003. Atmospheric mercury emissions from mine wastes and surrounding geologically enriched terrains. Environ. Geol. 43, 339–351.
Gustin, M.S., Rasmussen, P., Edwards, G., Schroeder, W., Kemp, J., 1999. Application of a laboratory gas exchange chamber for assessment of in situ mercury emissions. J. Geophys. Res. Atmos. 104, 21873–21878.
Hissler, C., Probst, J.L., 2006. Impact of mercury atmospheric deposition on soils and streams in a mountainous catchment (Vosges, France) polluted by chlor-alkali industrial activity: the important trapping role of the organic matter. Sci. Total Environ. 361, 163–178.
Jiskra, M., Wiederhold, J.G., Skyllberg, U., Kronberg, R.-M., Hajdas, I., Kretzschmar, R., 2015. Mercury deposition and re-emission pathways in boreal forest soils investigated with Hg isotope signatures. Environ. Sci. Technol. 49, 7188–7196.
Kinsey, J.S., Anscombe, F.R., Lindberg, S.E., Southworth, G.R., 2004a. Characterization of the fugitive mercury emissions at a chlor-alkali plant: overall study design. Atmos. Environ. 38, 633–641.
Kinsey, J.S., Swift, J., Bursey, J., 2004b. Characterization of fugitive mercury emissions from the cell building at a US chlor-alkali plant. Atmos. Environ. 38, 623–631.
Li, Z., Feng, X., Li, G., Bi, X., Zhu, J., Qin, H., Dai, Z., Liu, J., Li, Q., Sun, G., 2013. Distributions, sources and pollution status of 17 trace metal/metalloids in the street dust of a heavily industrialized city of central China. Environ. Pollut. 182, 408–416.
Li, Z.G., Feng, X.B., Li, G.H., Bi, X.Y., Sun, G.Y., Zhu, J.M., Qin, H.B., Wang, J.X., 2011. Mercury and other metal and metalloid soil contamination near a Pb/Zn smelter in east Hunan province, China. Appl. Geochem. 26, 160–166.
Lin, C.-J., Zhu, W., Li, X., Feng, X., Sommar, J., Shang, L., 2012. Novel dynamic flux chamber for measuring air–surface exchange of Hg^0 from soils. Environ. Sci. Technol. 46, 8910–8920.
Lin, C.J., Gustin, M.S., Singhasuk, P., Eckley, C., Miller, M., 2010. Empirical models for estimating mercury flux from soils. Environ. Sci. Technol. 44, 8522–8528.
Lin, H., Yuan, D., Lu, B., Huang, S., Sun, L., Zhang, F., Gao, Y., 2015. Isotopic composition analysis of dissolved mercury in seawater with purge and trap preconcentration and a modified Hg introduction device for MC-ICP-MS. J. Anal. At. Spectrom. 30, 353–359.
Lin, Y., Wang, S., Wu, Q., Larssen, T., 2016. Material flow for the intentional use of mercury in China. Environ. Sci. Technol. 50, 2337–2344.
Lindberg, S., Bullock, R., Ebinghaus, R., Engstrom, D., Feng, X.B., Fitzgerald, W., Pirrone, N., Prestbo, E., Seigneur, C., 2007. A synthesis of progress and uncertainties in attributing the sources of mercury in deposition. Ambio 36, 19–32.
Lindberg, S.E., Turner, R.R., 1977. Mercury emissions from chlorine-production solid-waste deposits. Nature 268, 133–136.
Lindberg, S.E., Zhang, H., Vette, A.F., Gustin, M.S., Barnett, M.O., Kuiken, T., 2002. Dynamic flux chamber measurement of gaseous mercury emission fluxes over soils: Part 2-effect of flushing flow rate and verification of a two-resistance exchange interface simulation model. Atmos. Environ. 36, 847–859.
Liu, J.L., Feng, X.B., Yin, R.S., Zhu, W., Li, Z.G., 2011. Mercury distributions and mercury isotope signatures in sediments of Dongjiang, the Pearl River Delta, China. Chem. Geol. 287, 81–89.
Moore, C.W., Castro, M.S., 2012. Investigation of factors affecting gaseous mercury concentrations in soils. Sci. Total Environ. 419, 136–143.
Obrist, D., Pokharel, A.K., Moore, C., 2014. Vertical profile measurements of soil air suggest immobilization of gaseous elemental mercury in mineral soil. Environ. Sci. Technol. 48, 2242–2252.
Pirrone, N., Cinnirella, S., Feng, X., Finkelman, R.B., Friedli, H.R., Leaner, J., Mason, R., Mukherjee, A.B., Stracher, G.B., Streets, D.G., Telmer, K., 2010. Global mercury emissions to the atmosphere from anthropogenic and natural sources. Atmos. Chem. Phys. 10, 5951–5964.
Ren, W., Duan, L., Zhu, Z., Du, W., An, Z., Xu, L., Zhang, C., Zhuo, Y., Chen, C., 2014. Mercury transformation and distribution across a polyvinyl chloride (PVC) production line in China. Environ. Sci. Technol. 48, 2321–2327.
Rothenberg, S.E., Mckee, L., Gilbreath, A., Yee, D., Connor, M., Fu, X.W., 2010. Wet deposition of mercury within the vicinity of a cement plant before and during cement plant maintenance. Atmos. Environ. 44, 1255–1262.
Schroeder, W.H., Munthe, J., 1998. Atmospheric mercury - an overview. Atmos. Environ. 32, 809–822.
Sommar, J., Zhu, W., Shang, L., Lin, C.J., Feng, X., 2016. Seasonal variations in metallic mercury (Hg^0) vapor exchange over biannual wheat–corn rotation cropland in the North China Plain. Biogeosciences 13, 2029–2049.
Southworth, G.R., Lindberg, S.E., Zhang, H., Anscombe, F.R., 2004. Fugitive mercury emissions from a chlor-alkali factory: sources and fluxes to the atmosphere. Atmos. Environ. 38, 597–611.
Tong, R.K., Yang, X.A., Li, Z.X., Luo, H.Y., Sun, Y.T., Li, F.S., Liu, L.L., 2000. Soil nutrient status and fertilization strategy of Hongda Tobacco in Kunming. Chin. Tobac. Sci. 3, 7–8.
Ullrich, S.M., Ilyushchenko, M.A., Kamberov, I.M., Tanton, T.W., 2007. Mercury contamination in the vicinity of a derelict chlor-alkali plant. Part I: sediment and water contamination of Lake Balkyldak and the River Irtysh. Sci. Total Environ. 381, 1–16.
Wang, D.Y., He, L., Shi, X.J., Wei, S.Q., Feng, X.B., 2006. Release flux of mercury from different environmental surfaces in Chongqing, China. Chemosphere 64, 1845–1854.
Wang, S.F., Feng, X.B., Qiu, G.L., Wei, Z.Q., Xiao, T.F., 2005. Mercury emission to atmosphere from Lanmuchang Hg-Tl mining area, Southwestern Guizhou, China. Atmos. Environ. 39, 7459–7473.
Wängberg, I., Edner, H., Ferrara, R., Lanzillotta, E., Munthe, J., Sommar, J., Sjöholm, M., Svanberg, S., Weibring, P., 2003. Atmospheric mercury near a chlor-alkali plant in Sweden. Sci. Total Environ. 304, 29–41.
Washburn, S.J., Blum, J.D., Demers, J.D., Kurz, A.Y., Landis, R.C., 2017. Isotopic characterization of mercury downstream of historic industrial contamination in the south river, Virginia. Environ. Sci. Technol. 51, 10965–10973.
Yin, R., Feng, X., Chen, B., Zhang, J., Wang, W., Li, X., 2015. Identifying the sources and processes of mercury in subtropical estuarine and ocean sediments using Hg isotopic composition. Environ. Sci. Technol. 49, 1347–1355.
Yin, R., Feng, X., Wang, J., Bao, Z., Yu, B., Chen, J., 2013. Mercury isotope variations between bioavailable mercury fractions and total mercury in mercury contaminated soil in Wanshan Mercury Mine, SW China. Chem. Geol. 336, 80–86.
Yin, R.S., Feng, X.B., Foucher, D., Shi, W.F., Zhao, Z.Q., Wang, J., 2010. High precision determination of mercury isotope ratios using online mercury vapor generation system coupled with multi-collector inductively coupled plasma-mass spectrometry. Chin. J. Anal. Chem. 38, 929–934.
Yu, B., Fu, X., Yin, R., Zhang, H., Wang, X., Lin, C.-J., Wu, C., Zhang, Y., He, N., Fu, P., Wang, Z., Shang, L., Sommar, J., Sonke, J.E., Maurice, L., Guinot, B., Feng, X., 2016. Isotopic composition of atmospheric mercury in China: new evidence for sources and transformation processes in air and in vegetation. Environ. Sci. Technol. 50, 9262–9269.
Zhang, H., Fu, X., Lin, C.J., Shang, L., Zhang, Y., Feng, X., Lin, C., 2016a. Monsoon-facilitated characteristics and transport of atmospheric mercury at a high-altitude background site in southwestern China. Atmos. Chem. Phys. 16, 13131–13148.
Zhang, H., Yin, R.S., Feng, X.B., Sommar, J., Anderson, C.W., Sapkota, A., Fu, X.W., Larssen, T., 2013. Atmospheric mercury inputs in montane soils increase with elevation: evidence from mercury isotope signatures. Sci. Rep. 3 https://doi.org/10.1038/srep03322.
Zhang, Y., Jacob, D.J., Horowitz, H.M., Chen, L., Amos, H.M., Krabbenhoft, D.P.,

Slemr, F., St. Louis, V.L., Sunderland, E.M., 2016b. Observed decrease in atmospheric mercury explained by global decline in anthropogenic emissions. Proc. Natl. Acad. Sci. U.S.A. 113, 526–531.
Zheng, W., Hintelmann, H., 2010. Nuclear field shift effect in isotope fractionation of mercury during abiotic reduction in the absence of light. J. Phys. Chem. A 114, 4238–4245.
Zhu, J.S., Wang, D.Y., Liu, X.A., Zhang, Y.T., 2011. Mercury fluxes from air/surface interfaces in paddy field and dry land. Appl. Geochem. 26, 249–255.
Zhu, W., Li, Z., Chai, X., Hao, Y., Lin, C.-J., Sommar, J., Feng, X., 2013a. Emission characteristics and air–surface exchange of gaseous mercury at the largest active landfill in Asia. Atmos. Environ. 79, 188–197.
Zhu, W., Lin, C.J., Wang, X., Sommar, J., Fu, X., Feng, X., 2016. Global observations and modeling of atmosphere–surface exchange of elemental mercury: a critical review. Atmos. Chem. Phys. 16, 4451–4480.
Zhu, W., Sommar, J., Li, Z., Feng, X., Lin, C.-J., Li, G., 2013b. Highly elevated emission of mercury vapor due to the spontaneous combustion of refuse in a landfill. Atmos. Environ. 79, 540–545.
Zhu, W., Sommar, J., Lin, C.J., Feng, X., 2015a. Mercury vapor air–surface exchange measured by collocated micrometeorological and enclosure methods - Part I: data comparability and method characteristics. Atmos. Chem. Phys. 15, 685–702.
Zhu, W., Sommar, J., Lin, C.J., Feng, X., 2015b. Mercury vapor air–surface exchange measured by collocated micrometeorological and enclosure methods – Part II: bias and uncertainty analysis. Atmos. Chem. Phys. 15, 5359–5376.
Zhu, W., Song, Y., Adediran, G.A., Jiang, T., Reis, A.T., Pereira, E., Skyllberg, U., Björn, E., 2018. Mercury transformations in resuspended contaminated sediment controlled by redox conditions, chemical speciation and sources of organic matter. Geochim. Cosmochim. Acta 220, 158–179.